Available online at www.sciencedirect.com
SCIENCE DIRECT
ELSEVIER
Icarus 181 (2006) 465–474
ICARUS
www.elsevier.com/locate/icarus

A model of the ionosphere of Saturn's rings and its implications

J.G. Luhmann [a,*], R.E. Johnson [b], R.L. Tokar [c], S.A. Ledvina [a], T.E. Cravens [d]

[a] *Space Sciences Laboratory, University of California, 7 Gauss Way, Berkeley, CA 94720, USA*
[b] *Materials Science and Engineering, University of Virginia, Charlottesville, VA 22904, USA*
[c] *Los Alamos National Laboratory, Los Alamos, NM 87545, USA*
[d] *Department of Physics and Astronomy, University of Kansas, Lawrence, KS 66045, USA*

Received 30 June 2005; revised 21 October 2005

Available online 30 January 2006

Abstract

The detection of cold O_2^+ and O^+ ions in the vicinity of Saturn's rings during the Cassini Orbiter orbit insertion confirmed expectations that the rings would have a water product atmosphere and ionosphere. These observations prompted a new look at their origin and nature by Johnson et al. [Johnson, R.E., Luhmann, J.G., Tokar, R.L., Bouhram, M., Berthelier, J.J., Sittler, E.C., Cooper, J.F., Hill, T.W., Crary, F.J., Young, D.T., 2006. Icarus 180, 393–402], but also raised questions about the ionosphere's spatial distribution and fate that inspired the ionospheric model described in this report. Here a test particle model with some Monte Carlo aspects is used to consider the behavior of the O_2^+ and O^+ ions produced in the atmosphere of Saturn's rings. Key features of these calculations include the Johnson et al. description of the production of the ring atmosphere, and the effects of the offset dipole magnetic field of Saturn. The results suggest that the latter should produce some possibly observable asymmetries in both the inner ring ionosphere and the precipitation of ring ions into the atmosphere of Saturn. Further in situ observations of the rings are not currently planned, but remote sensing instruments on Cassini may provide future observational tests of the model.

Keywords: Atmospheres, dynamics; Ices; Planetary rings; Saturn; Saturn, magnetosphere

1. Introduction

The rings of Saturn are composed of dust and dirty water ice bodies of up to boulder size (e.g., Esposito et al., 2005). These are exposed to sunlight, both direct and reflected from Saturn or other parts of the rings themselves, as well as the magnetospheric and ionospheric electron and ion populations, and neutral particles. All of these are potential sources of a gaseous atmosphere of the rings. Models of the atmosphere of the rings (Ip, 1984, 1995; Pospieszalska and Johnson, 1991) have predicted the presence of H_2O, O_2, O, OH, H from meteoroid impacts and photo-desorption and/or energetic particle sputtering of ring material, while the Hubble Space Telescope detected an extended OH cloud (Shemansky et al., 1993; Jurac et al., 2002) that appeared to reach into the region occupied by the rings (∼1.4–2.4 R_S, equatorial). Thus the Cassini Orbiter observations during Saturn orbit insertion (SOI) sparked renewed interest in the environment of the rings, and the effects of their interaction with the surrounding particles and fields.

Low energy ion composition detection techniques are generally more sensitive than current neutral particle detectors such as gas mass spectrometers. Two instruments on the Cassini Orbiter that are capable of in situ detection of rarefied atmospheres through detection of their ionospheres are the ion and neutral mass spectrometer (INMS) (Waite et al., 2005) and the Cassini plasma analyzer (CAPS) (Young et al., 2005). Together, these can sense heavy ions at low energies (several eV to 10s of keV) down to densities of $\sim 10^{-2}$ cm^{-3} (CAPS) and $\sim 10^{-4}$ cm^{-3} (INMS), provided that their apertures or fields of view are suitably oriented. Both INMS and CAPS detected O_2^+ and O^+ ions in the minutes prior to and following the descending ring plane crossing at distances of ∼1.8–2.1 R_S (CAPS), and ∼2.3–3.0 R_S (CAPS and INMS). These intervals were determined in large part by the instruments' pointing and operation modes, and so do not preclude the existence of ring ions over a broader range

* Corresponding author. Fax: +1 (510) 643 8302.
E-mail address: jgluhmann@ssl.berkeley.edu (J.G. Luhmann).

0019-1035/$ – see front matter
doi:10.1016/j.icarus.2005.11.022

of locations. The availability of observations raised new challenges for models of the ring atmosphere and ionosphere.

One problem is that the energetic particle population detected during Cassini SOI drops rapidly near the outer edge of the rings at about 2.3 R_S, although it reappears inside of the main rings (∼1.4 R_S) (Krimigis et al., 2005). These observations confirm the expectation that the rings absorb the charged particles as they radially diffuse inward and bounce between the northern and southern hemispheres in Saturn's nearly dipolar magnetic field. As they are absorbed at the outer edge of the rings, the energetic particles must produce a component of the atmosphere of the rings by particle sputtering. However, away from the ring boundaries, once the energetic particles are absorbed, their contribution as a source disappears. If the atmosphere of the rings extends over a large radial extent, as the Cassini INMS and CAPS observations suggest, there must be other sources and/or ion redistribution processes.

The ring ionosphere, by virtue of its greater detectability on Cassini, provides indirect confirmation of a ring atmosphere's existence. The neutral atoms and molecules can be ionized by either direct or reflected sunlight, by magnetospheric electron impact ionization, or by charge exchange with ions in the neighborhood. The detected species O_2^+ suggests the presence of a molecular oxygen atmosphere. HST (Hall et al., 1995) and the Galileo spacecraft UV investigation (Hansen et al., 2005) observed an O_2 atmosphere around Jupiter's icy satellite Europa whose source was suggested to be energetic ion and electron impact-induced decomposition of ice (Johnson et al., 2003; Shematovich et al., 2005). It was recently suggested that this same basic process may be at work in Saturn's rings, but dominated by UV photon-induced decomposition (Johnson et al., 2006). Further details on the rarefied neutral atmosphere of the rings from Cassini depend in part on our ability to interpret the ionospheric observations.

The ring ionosphere is also interesting in its own right. Ring atmosphere ions can be accelerated to greater than escape velocities by the corotation electric field of Saturn, and following neutralization by charge exchange with surrounding neutrals, escape into the outer magnetosphere or even interplanetary space. Thus the ring ionosphere is an important part of the chain of mass production in, and escape from, Saturn's magnetosphere. The observed spatial extent of the ring ionosphere is also interesting in light of the Voyager era report that the aligned nearly ideal dipole field of Saturn is offset with respect to the planet's gravitational center by ∼0.04 R_S toward the north, along the rotation axis (Connerney et al., 1983). This offset, which has now been confirmed by the Cassini magnetometer team (Dougherty et al., 2005) should in part dictate the latitudinal extent and symmetry of the ring ionosphere "ion torus" as the produced ions mirror about the magnetic equator lying above the ring plane. Inferred small axisymmetric higher order moments should not significantly affect the ion motions near the equator. The ring ionosphere is thus also a diagnostic for Saturn's internal magnetic field irregularity and its consequences.

In this report we examine some of the expected consequences of the ion production process and the offset dipole for the characteristics of Saturn's ring ionosphere using a simplified test particle model. In particular, we show that the combination of the gravitational field and the corotation electric field acting on the ring ions in the offset dipole field may produce asymmetries in both the ring ionosphere and its interaction with Saturn's atmosphere. Our model is consistent with the Cassini SOI observations by INMS and CAPS, and also predicts features beyond those that can be verified with the available limited observations. Although the Cassini Orbiter will not approach the ring radial distances again during its prime mission, the possible remote observations of the ring atmosphere and ionosphere by Cassini instruments through their ultraviolet emissions (Esposito et al., 2005), and via energetic neutral atoms (ENA) arising from energetic particle charge exchange with the neutrals in Saturn's magnetosphere (Krimigis et al., 2005), may provide further tests of the model and its implications.

2. A model of the ring ion source

As mentioned above, the Cassini observations of mainly O_2^+ ions are consistent with a Europa-like mainly O_2 atmosphere. The ultimate ion source rate for the rings is due to photoionization with a branching ratio, a measure of relative production rate, for O_2^+ and $O + O^+$ that favors O_2^+ by a ratio of about 4–1. The O_2^+ ions are produced as cold (∼100–200 K or ∼0.01–0.02 eV) ions while the latter process makes hot O^+ ions and hot neutral O (∼0.5–1 eV each). The setting of the rings is such that ions created near the ring plane are "picked up" with an initial Keplerian velocity for the radial distance of their parent neutrals from Saturn, plus a small velocity component from the ion creation process (Johnson et al., 2006). At these low energies, the ions are controlled by the combination of the nearly dipolar local magnetic field, the corotation electric field, and Saturn's gravitational field.

The cold O_2^+ thermal velocity plus the corotation velocity gained from the electric field result in a flat angular distribution. Therefore the O_2^+ is injected nearly along the ring plane, while the suprathermal O^+ is more isotropically injected. After injection the ions are subject to further interaction with the rings and the ring atmosphere. Because the cold ions must mirror close to the ring plane, they spend much of their time in the neutral ring atmosphere. As a consequence, both the O_2^+ and O^+ ions are likely to undergo one or more collisions with neutral O_2 molecules before returning to the ring plane. The collisions produce scattered ion populations with higher parallel (to the magnetic field) velocities so that they mirror farther from the ring plane than they would in the absence of the collisions. Whether a collision results in a gain or loss of energy for the ion or the neutral is determined by the complex interplay of forces on the particles in this region of Saturn space. Any ring atmosphere neutrals that are energized by collisions with ions that have gained energy from the corotation electric field can also be photoionized outside of ring plane, providing an extended source of new, more energetic pickup ions at larger radial distances (>2.4 R_S). However, here we do not consider this secondary potential source of new ions, but instead con-

centrate on the fate of the primary ion population born in the rings.

An interesting aspect of the ring ionosphere that merits exploration is the effect of the dipole field offset mentioned earlier. The ∼0.04 R_S northward displacement of the dipole field with respect to Saturn's rotational equator should cause most of the newly created ions to experience an initial northward mirror force near the ring plane. Ions originating over the southern face of the rings are thus more quickly reflected back into the rings, while in the north, the ions can be trapped around the magnetic field minimum of the dipole equator if a scattering collision increases their pitch angle. Thus the potential residence time and hence density of ions produced over the north face may be larger than over the south face of the rings. In addition to the magnetic mirror forces, gravity is always acting on the ions. The rings span the interesting radius, at ∼1.8 R_S, where the Keplerian velocity is equal to the corotation velocity. As a result, the traditional picture of ion tori energized by the corotation electric field does not hold equally throughout the ∼1.4–2.4 R_S radial range of the rings. To examine the implications we construct a model which includes the essential geometrical and physical elements of the ring ions' setting.

A ring ionosphere model is generated by following mass 32 and 16 amu singly ionized test particle ions injected at 0.2 R_S intervals between 1.4 and 2.4 R_S on a radial grid. We numerically solve the full ion equation of motion $m\bar{\mathbf{a}} = q(\bar{\mathbf{E}} + \bar{\mathbf{v}} \times \bar{\mathbf{B}})$ (where m is ion mass, $\bar{\mathbf{a}}$ is the ion acceleration, q is the single electron charge of the ion, $\bar{\mathbf{v}}$ is the ion velocity, and $\bar{\mathbf{E}}$ and $\bar{\mathbf{B}}$ are the magnetospheric electric and magnetic fields with $\bar{\mathbf{E}}$ equal to the corotation field $\bar{\mathbf{E}} = -(\bar{\mathbf{V}} \times \bar{\mathbf{B}})$ with $\bar{\mathbf{V}}$ the local magnetospheric corotation velocity). The dipolar magnetic field $\bar{\mathbf{B}}$ includes a dipole moment offset along the spin axis of $z = +0.04$ R_S (where the z axis is the spin axis). The corotation electric field is consistent with Saturn's rotation period of ∼10.2 h. The Saturn-centered gravitational field is consistent with the mass of Saturn. No attempt is made to simulate the Cassini Gap or other ring gaps in this first-order model. The use of a radial grid introduces a small (factor of ∼2) initial weighting function per unit area of ring surface that decreases with radius. This has only a minor effect on the overall statistics, and can eventually be made more precise once the details of the ion production mechanism(s) are more fully worked out.

The present model is also not steady state, in the sense that rates of ion production and loss are not forced to balance. Ion injections along a single radial rapidly populate all azimuths during each model calculation run, after which the gross appearance of the results do not change appreciably with run time.

Angular distributions of the injected ions are approximated by injecting 100 particles at each injection point, with a directional distribution mimicking an initially flat or isotropic injection, depending on whether the ion species is O_2^+ or O^+. We further assume ion–neutral collisions occur in a layer of ambient neutrals centered on the ring plane so that ions can be scattered once they leave the plane. They are assumed to be absorbed at the ring plane when they return, at which time a new ion is launched to maintain a steady test particle population. The ion–molecule collisions with the ambient O_2 molecules are treated in a quasi Monte Carlo fashion with random pitch angle cosine changes and center of mass energy redistributions at time intervals determined by the estimated collision frequency. The O_2 was assumed to exist in a uniformly dense layer 1000 km thick on either side of the ring plane (the approximate scale height derived by Johnson et al., 2006). No other spatial or energy diffusion mechanisms are included in the present model.

A standard energy-conserving finite difference method is used to solve the ion equation of motion of each injected particle. Time steps of 0.01 gyroperiod assure an accurate solution over the long time of each integration. The results are based on particles followed for 12 million time steps, with their positions registered every 120,000 time steps. Because the time step is fixed and uniform, the statistics of the ion locations can be used to visualize densities and calculate energy and angular distributions. The primary results are illustrated by Figs. 1–10.

3. Results

Figs. 1a, 1b show the locations of O_2^+ and O^+ ions, respectively, obtained under the above assumptions for the forces on the particles and the neutral density-related ion–molecule collision process. Without the ion–molecule collisions the latitudinal distributions of the ions would be largely confined to the space $z = 0$–0.08 R_S, north of the ring plane and centered on the magnetic equator at $z = +0.04$ R_S. The much broader latitudinal distribution is the result of collisions re-orienting the trajectories of the ions from those they would have from their initial Keplerian velocity and corotation electric field pickup alone. These snapshots of the calculated ion positions show a few modeling artifacts from the 0.2 R_S separation of the injection radii, which is much larger than the ion gyroradius. Nevertheless, the bouncing motion between mirror points in the northern and southern dipole hemispheres is clearly seen. The displacement of the bounce motion symmetry plane northward of the ring plane is less clear in these displays, but its effects become apparent below. Given the collision times for O_2^+ of $\sim 10^4$ s (2.8 h) and O^+ of $\sim 1.4 \times 10^4$ s (3.9 h), a few direction and energy altering collisions will occur before a particle injected from the ring plane returns to the ring plane. These collisions are what populate the latitudes above a few degrees with ions, producing the effective scale height of the ionosphere.

Fig. 1c shows a view of the modeled ion trajectories projected onto the x–z plane of symmetry. Because the gyroradii of the ions are small compared to the system under consideration (a mass 32, singly ionized 10 eV ion has a gyroradius of ∼0.5 km in a 5000 nT field), they effectively delineate the dipolar field lines on which they are injected. A striking change of ion behavior occurs at $R \sim 1.8$ R_S, the approximate radius where Keplerian and corotation velocities are equal. The ions inside of this radius, $R = R_x$, travel much further along the dipolar field lines from their ring source than ions outside of $R = R_x$. Moreover, they spiral into the atmosphere of Saturn, primarily in the southern hemisphere.

Fig. 1d shows the contrasting case of projected O_2^+ ion trajectories in the offset dipolar field, but without the ion–molecule collision scattering. The effective ion scale height is much re-

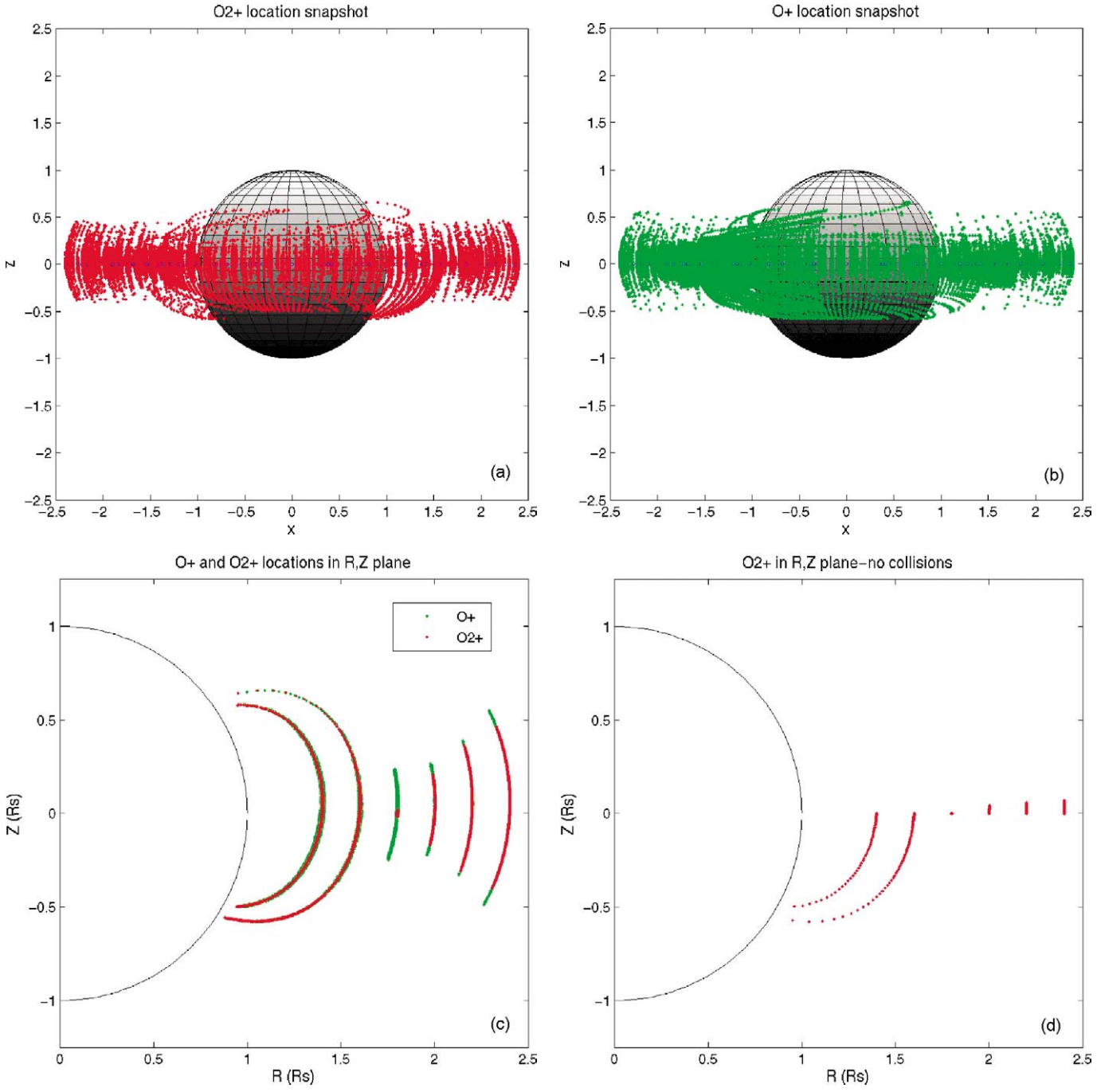

Fig. 1. (a) Locations of O_2^+ ion locations in the model. The inner layers of the ring ionosphere can be seen to extend to higher and lower latitudes than the outer layers, with more of the ions in the south. These ions precipitate into Saturn's atmosphere. (b) Same as (a) but for O^+. (c) Trajectories projected into a meridian plane to illustrate the effective "scale heights" of the ions versus equatorial radius. The radial gaps are the result of the starting point grid spacing. (d) Same as (c) for O_2^+ but without scattering by ion–molecule collisions.

duced outside $R = R_x$, where it is determined mainly by the $\sim$0.04 R_S dipole offset to the north of the ring plane. Inside $R = R_x$ the results are similar to those shown in Fig. 1c, but the ion precipitation along the field lines is confined to the southern hemisphere.

To further understand this behavior we performed a numerical experiment in which an ion was introduced into a simple axial magnetic mirror geometry, with an externally imposed force of specifiable strength and direction along the mirror field axis. Two strong field regions at either end of the experiment volume formed an effective ion trap for ions injected near the midplane. The effect of gravity in Saturn's offset dipole field was approximated by an external field that changed direction at a point along the mirror axis, which was moved away from the mirror center. (In the rings, the radial force of Saturn's gravity, pulling particles down the dipolar field lines, competes with the mirror force near their mirror points, which pushes them upward toward the magnetic equator.) We determined that for

circumstances similar to those in the inner magnetosphere of Saturn (the presence of an axial external force directed away from a point near, but not at, the mirror's center, opposing the mirror force at both ends), an initially trapped ion can leave the trapping region within a bounce period. Thus the radial force of Saturn's gravity on the ion, coupled with Saturn's dipole magnetic field, can cause an otherwise trapped ion to precipitate into Saturn's atmosphere. The preference for the "leakage" from the side of the mirror containing the centroid of the external force was also seen in the aforementioned numerical experiment. The occurrence of the leakage depends on the relative strength of the external force and the mirror force. Outside of $R = R_x$ the gravitational field effect becomes negligible compared to the mirror force, and the particles remain trapped unless they are scattered into the loss cone by the ion–molecule collisions or another process (e.g., wave–particle interactions) that is not included in the present model.

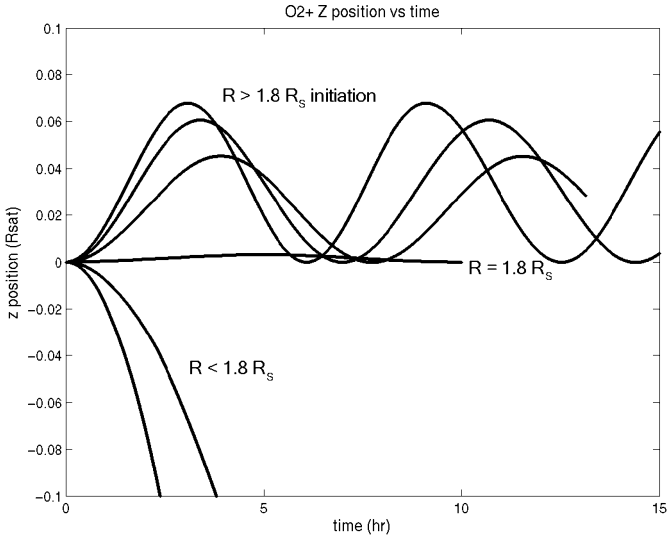

Fig. 2. Time history of the z (north–south) coordinate for single test O_2^+ ions launched at $R = 1.2, 1.4, 1.6, 1.8, 2.0, 2.2, 2.4\ R_S$. The ions launched outside of 1.8 R_S are magnetically trapped and mirror between the northern and southern hemispheres in the displaced dipole field. For these radial distances the bounce periods are ∼6–8 h. The ion at 1.8 R_S moves almost without displacement from its Keplerian motion. The ions inside of 1.8 R_S "fall" into the southern Saturn hemisphere.

We also co-located the dipole and rotational equators in a run of the full Saturn model and observed no detrapping of the ions injected at $R < R_x$ in that case. In addition, we moved the dipole equator to the opposite side of the ring plane and obtain the expected reversed north–south asymmetry of the behavior of ions injected at $R < R_x$. The ions' behavior is further understood by examining time histories of the calculated positions in z of six test O_2^+ ions launched from the ring plane ($z = 0$) at $R = 1.4, 1.6, 1.8, 2.0, 2.2, 2.4\ R_S$, without the complication of the ion–molecule collisions, as shown in Fig. 2. The ions launched at $R > R_x$ bounce between mirror points in z with a period of ∼6–8 h. The ion launched near R_x (≈1.8 R_S) shows almost no evidence of ion-pickup induced motion, as would be expected given that the convection electric field is nearly zero in that ion's Keplerian speed reference frame. The ions launched inside R_x vanish off the bottom of the plot as they fall into Saturn's atmosphere. These results suggest that gravity destabilizes the trapping of the ring ions with an onset of the instability at $R = R_x$.

The interplay between the corotation electric field and gravity in controlling the motion of the ions is better seen by plotting their velocities at the positions shown in comparison with the Keplerian speed and corotation speed versus the radial distance R. Figs. 3a, 3b show the O_2^+ and O^+ test particle velocities at the positions in Figs. 1a, 1b. The spreads of the locations inward of the initial radial distances result from the ion–molecule collisions, and, at $R < R_x$, from the gravitational field effect on the ring ions inside $R = R_x$. The ions start with the Keplerian velocity but are affected by the corotation elec-

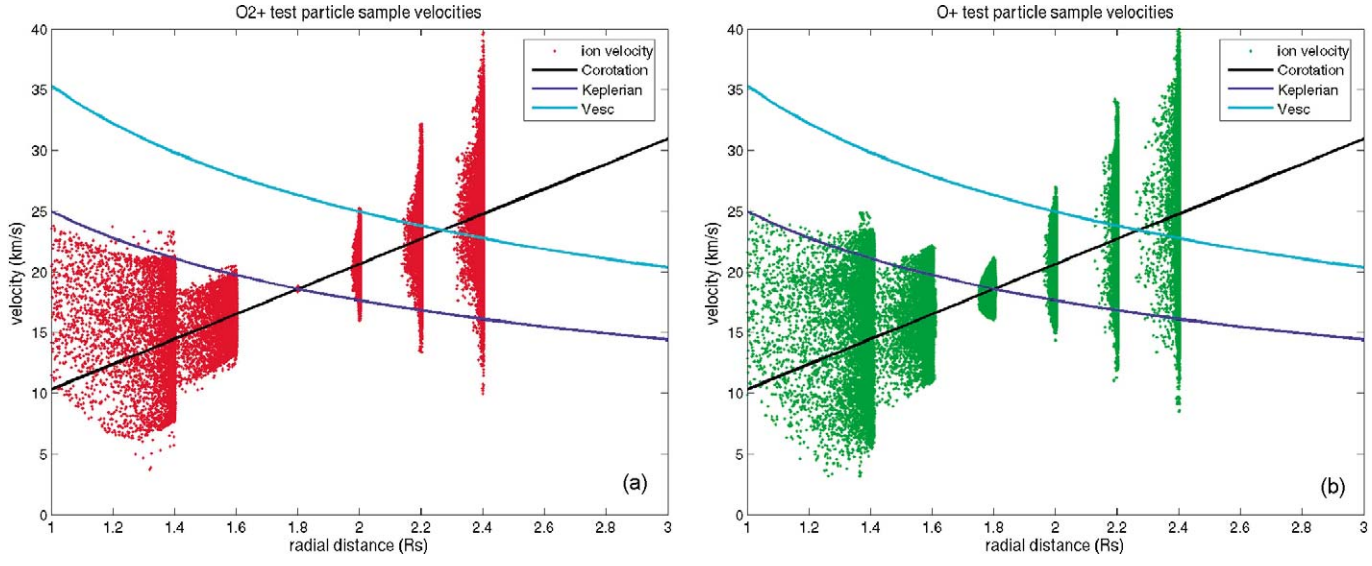

Fig. 3. (a) Calculated O_2^+ velocities from the model as a function of radial distance from Saturn. The radial separations of clusters of points reflect the selected launch points. The behavior of the ions results from the combined pickup and scattering processes, but inside of the radius where the Keplerian and corotation speeds are equal, the greater effect of gravity is seen. The escape velocity is also shown. (b) Same as (a) but for O^+.

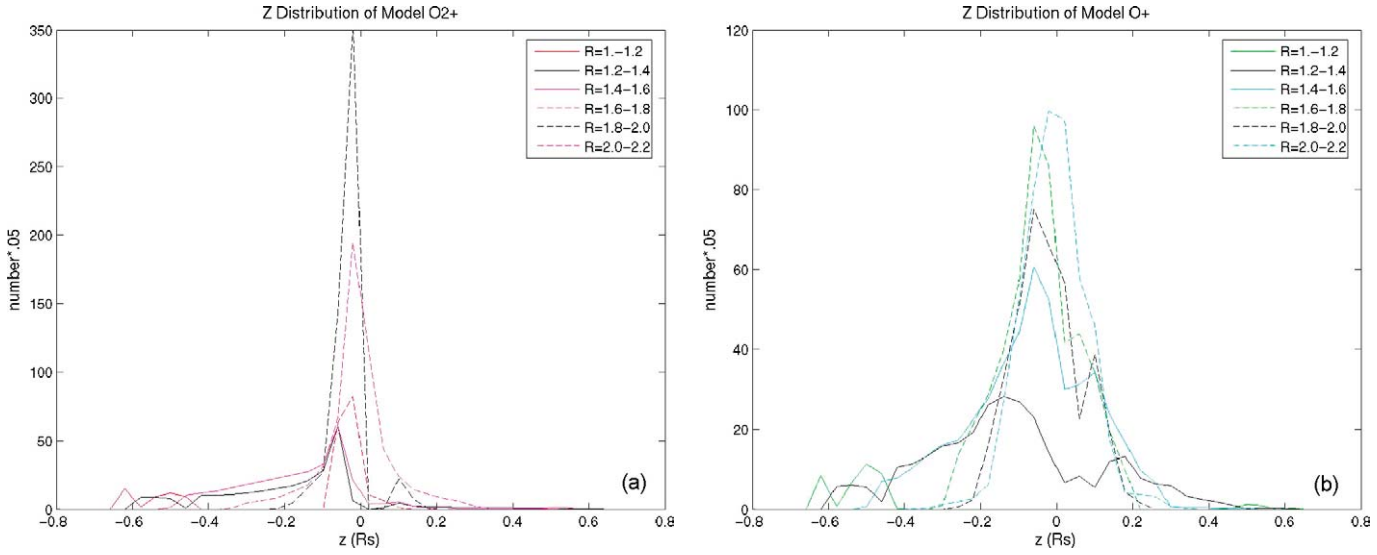

Fig. 4. Statistics of the z coordinates of the test particles in Figs. 1a, 1b, showing the effective scale heights due to the magnetic mirroring and assumed scattering processes. (a) For O_2^+ and (b) for O^+.

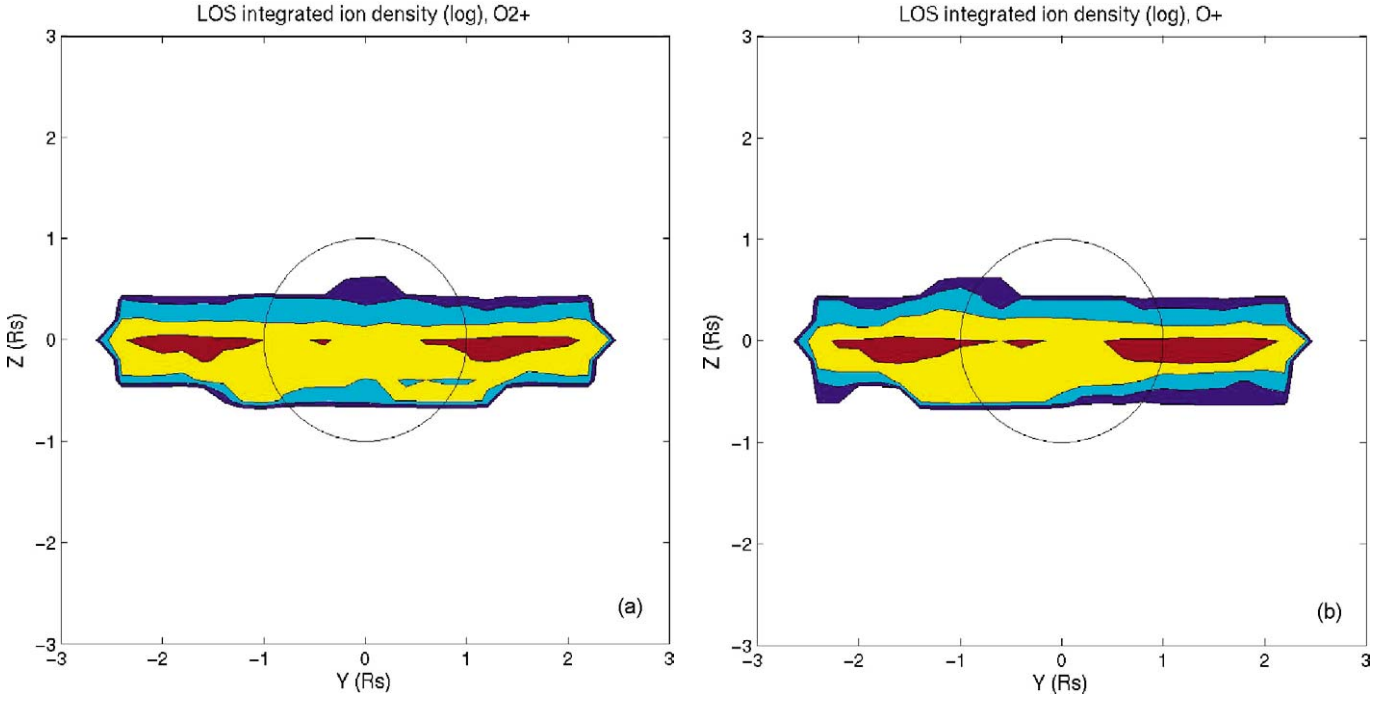

Fig. 5. (a) Contours of effective O_2^+ and (b) O^+ densities (arbitrary units, log 10 contours) derived from the statistics of the points in Figs. 1a, 1b.

tric field in such a way that, in the absence of collisions, they oscillate between $V = V_{\text{kep}}$ and $V = 2V_{\text{cor}} - V_{\text{kep}}$. This oscillating motion is consistent with the effect of the corotation electric field, which is to maintain the ion gyrocenter motion at V_{cor}, regardless of the initial velocity. However, with collisions, the velocity range is increased and spreads, and gravity alters this simple behavior noticeably at $R < R_x$. Note that some of the ions exceed the escape velocity at radial distances greater than $\sim$2.1 R_S, so if these become neutralized by charge exchange they can escape from Saturn, or at least into the magnetosphere, depending on their direction and the probability of further charge transfer collisions.

Some statistics of the results are given in Figs. 4a, 4b which show the effect of the dipole offset on the scale heights (in distance above the ring plane, z) of O_2^+ and O^+. The statistics are sorted by radial distance to show the behavior also illustrated by Fig. 1c. North–south differences in scale height are most apparent inside $R = R_x$, consistent with the dynamics of the particles described above. The O^+ ions in Fig. 4b have generally larger scale heights that the O_2^+ ions in Fig. 4a because of their higher initial energies. In Figs. 5a, 5b the results in Figs. 1a, 1b are turned into integrated line of sight density (arbitrarily normalized) contours. Similar statistics in the plane of symmetry (r–z plane) are shown in Figs. 6a, 6b. These give an

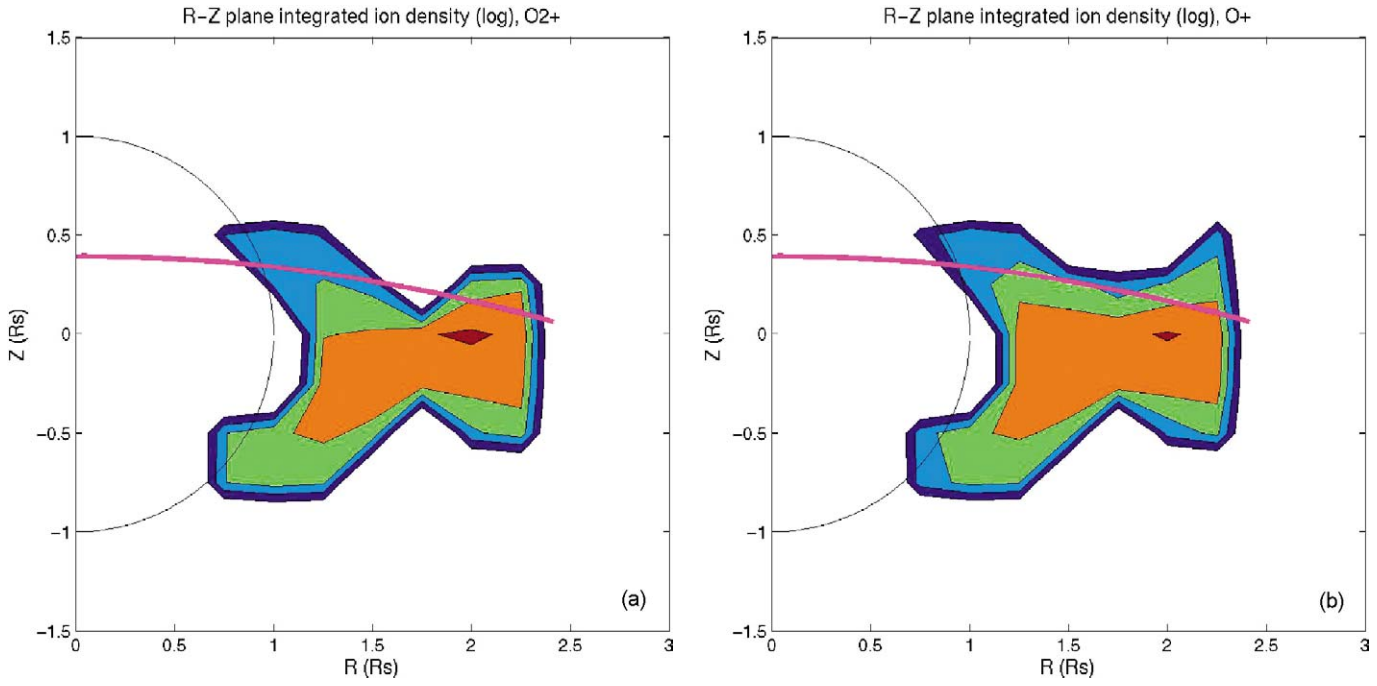

Fig. 6. Same as (a) Fig. 5a (O_2^+) and (b) Fig. 5b (O^+), but in the r–z plane. For reference, the projection of the Cassini Orbiter SOI orbit segment is shown superposed.

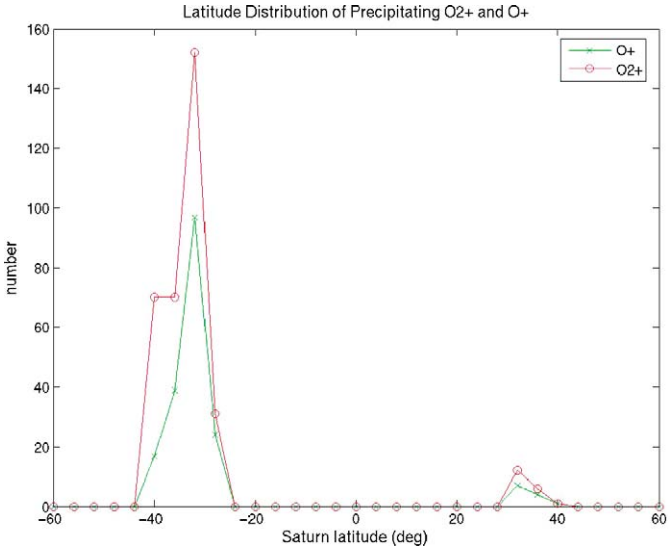

Fig. 7. Illustration of the latitude distribution of the precipitating ions, showing the north–south asymmetry related to the dipole field offset.

idea of how each ion torus might look if the ions emitted photons at some remotely detectable wavelength. Note that because the magnitude of the dipole equator northward shift is small on these global scales, its effect appears mainly as north–south asymmetries. The locations of the precipitating ions are another possible place where emissions can be excited. Fig. 7 shows the inferred latitude distribution of the precipitating ring ions, which could in fact be broadened by some inward radial diffusion process not included here. The fact that these ions reach the atmosphere also prompted us to add an effective ambipolar electric field correction to the forces on the ions. This polarization electric field is expected to exist in the upper atmosphere of Saturn as a result of the differential effect of gravity on Saturn's own ionospheric electrons and ions (e.g., Wilson, 1991). The addition of this field, which effectively reduces the mass of the ion by a factor ∼2, has little difference on the overall results. Fig. 8a shows the energy spectrum derived from all of the ions in the modeled torus, and Fig. 8b shows the spectrum of the precipitating ions for contrast. The low energies of the precipitating ions suggest they will mainly affect Saturn's upper atmosphere. Approximately one percent of the ions shown in Figs. 1a, 1b suffer this fate. If $\sim 10^{27}$ s^{-1} are produced by the rings, as some authors suggest (e.g., Johnson et al., 2006), one can calculate the flux into the southern latitude band in Fig. 7.

It is also of interest to examine the ion energy spectra as a function of radial distance. Figs. 9a, 9b show the statistics of the test particle energies in various radial ranges in the model. The effect of an increasing corotation speed with radius on the ion energies is seen, but there is also an increasing width of the spectrum. This latter effect occurs as the pickup process becomes more classical: as the corotation velocity exceeds the Keplerian speed by increasing amounts, an observer will detect a broader range of energy oscillation between the initial Keplerian speed and energy equivalent to twice the corotation speed. Another useful display is the pitch angle distribution of the ions, which is shown in Figs. 10a and 10b, this time for all spatial locations but sorted by ion energy. Even with the pitch angle scattering associated with the ion–molecule reactions in the model, the ions largely preserve pickup ion-like distributions peaking near 90°. The few degree offsets of the peaks from 90° can be attributed to the pickup of the ions near the ring plane source located off the dipole equator.

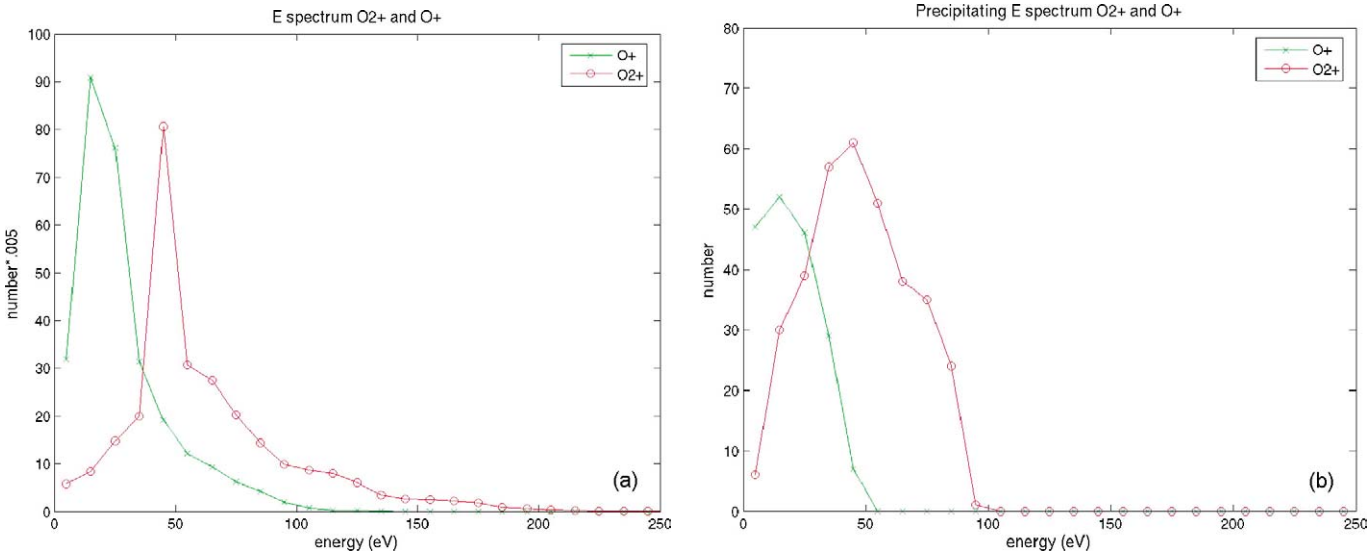

Fig. 8. (a) Calculated ion energy spectra for the entire modeled ion populations. (b) Energy spectra of the precipitating component just prior to impacting the planetary boundary.

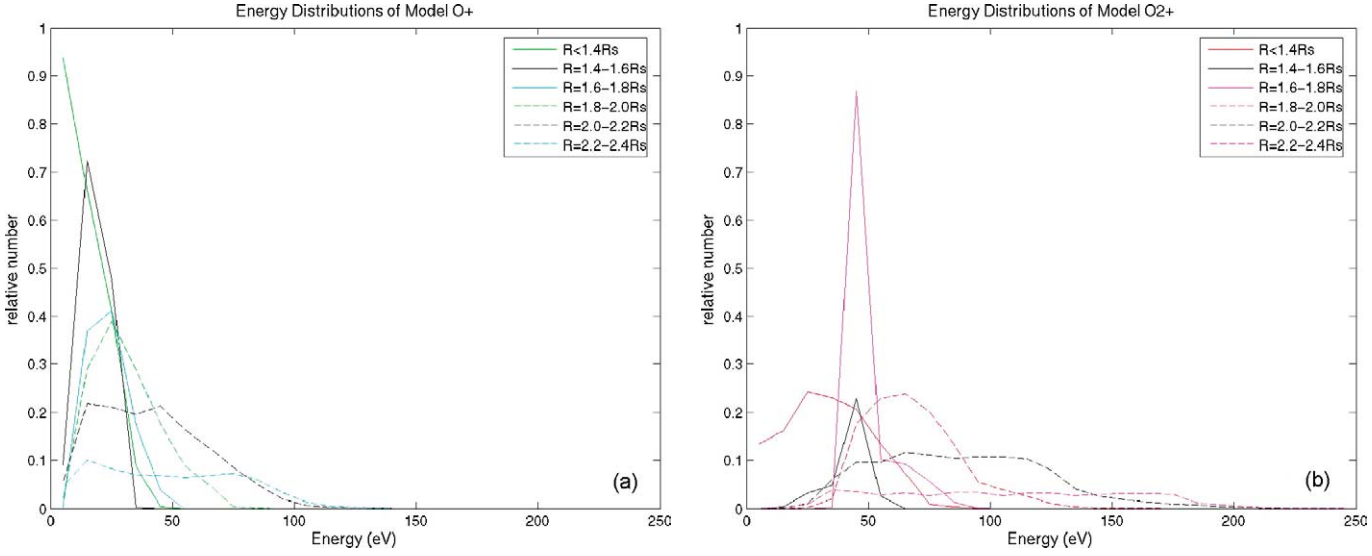

Fig. 9. (a) Calculated ion energy spectra for O_2^+ obtained from the statistics of the test particles in various radial distance ranges of the model. (b) Same as (a) but for O^+.

4. Discussion

The calculations described here simulate what might be observed at Saturn, by low energy ion instruments such as Cassini CAPS and INMS, in the vicinity of Saturn's rings. The interpretation of these ion data in terms of the neutral atmosphere of the rings, and also in terms of the effects of the ring atmosphere on the magnetosphere, requires detailed modeling that takes into account the forces that control the particles. Here we assumed a neutral particle distribution based on work described elsewhere (Johnson et al., 2006) and focused on the question of how the ring ionosphere is formed, interacts with the ambient atmosphere, and behaves in the force field environment of the rings. We find some potentially significant results which could not have been anticipated without such modeling. One is that the ions inside of the radial distance where the Keplerian and corotation velocities are equal ($R_x \approx 1.8\ R_S$) are noticeably affected by Saturn's gravitational field compared to ions outside this radius. The combination of the planet's dipole field offset from the planet's gravitational center leads to a preferential precipitation of ring ions into the southern hemisphere of Saturn, at a latitude of about 30°. The ring ionosphere therefore undergoes a drastic transition inside of that radius, R_x, extending along the dipole field lines with a large scale height. The other consequence is that the ring ion torus is globally asymmetric between the northern and southern hemispheres, with a larger southern hemisphere density inside $R < R_x$. We have not examined the possible consequences for the neutral ring atmosphere and neutral escape.

Do reported Cassini results show any evidence of these attributes? Thus far the only detail has been provided by the in situ SOI results from CAPS and INMS. Both of these instruments detected the species O_2^+ and O^+ ions examined here within the spatial domains of the model, though their sam-

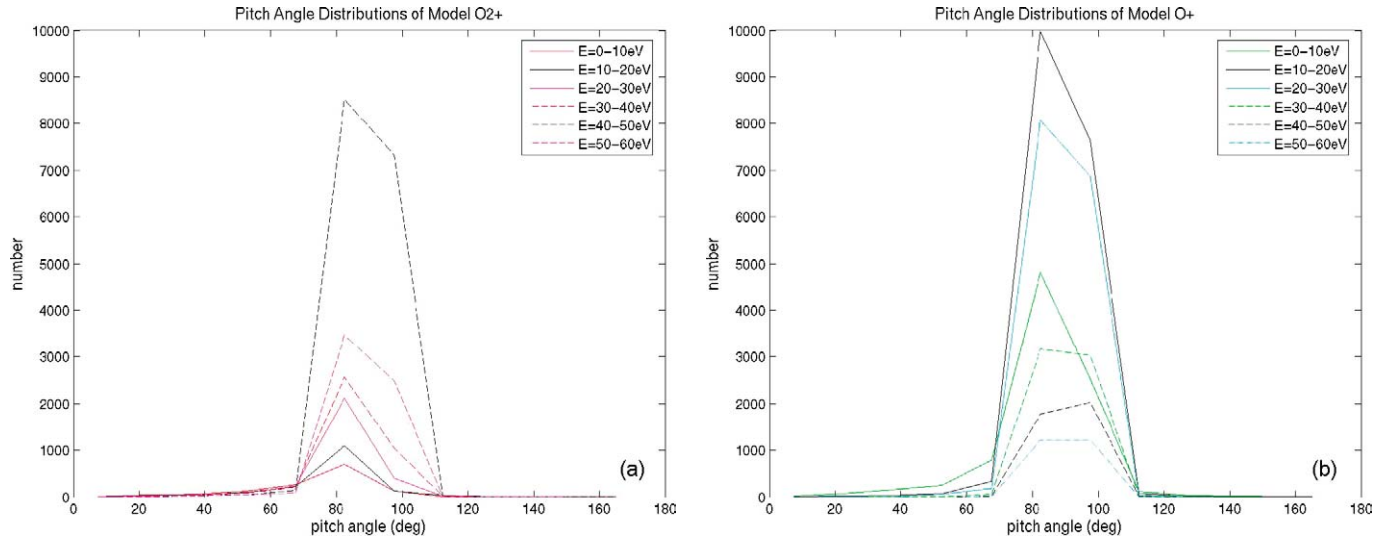

Fig. 10. (a) Calculated pitch angle distributions for O_2^+ at various energies, for the entire spatial domain of the model. (b) Same as (a) but for O^+.

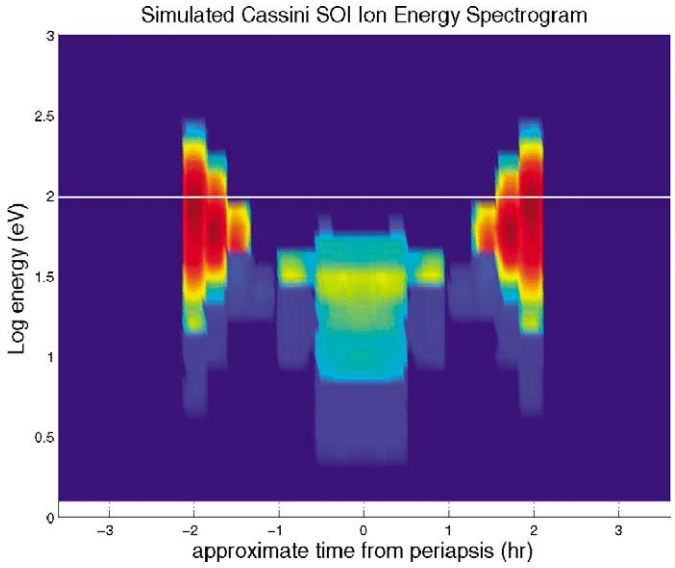

Fig. 11. Simulated SOI ion energy spectrogram calculated by "flying through" the model along the SOI trajectory (see Fig. 6 showing the outbound portion; inbound is nearly symmetrical). This spectrogram shows the ion energies in the rest frame of Saturn, with the INMS energy limit indicated by the horizontal line. The color scale is a linear "counts" or ion number scale. The samples around $R = 1.8\ R_S$ have small numbers because of the thinness of the ring ionosphere in this region, combined with the SOI trajectory. Both O_2^+ and O^+ are included in this spectrogram, with the O_2^+ multiplied by a factor of 4 to account for its greater production rate (see text). It is difficult to distinguish the O^+ peaks in this display, which uses logarithmic energy bins of 0.1. The raggedness of the spectrogram is an artifact of the model's 0.2 R_S separated injection radii.

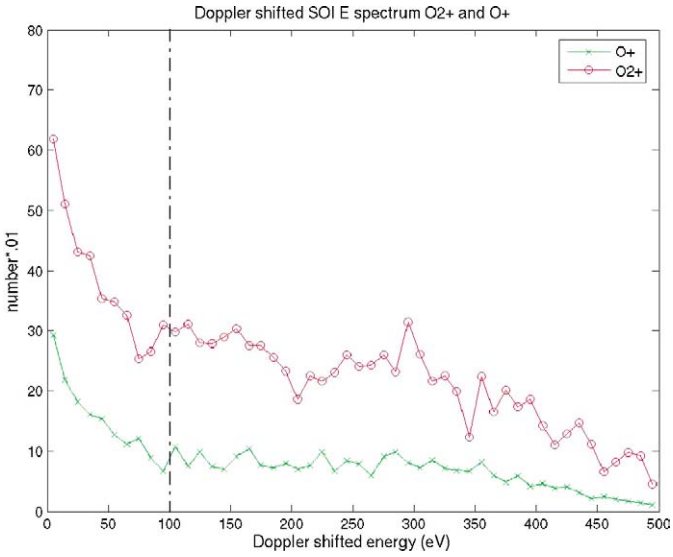

Fig. 12. Doppler shifted ion energy spectra for the model O_2^+ and O^+ populations sampled along the SOI trajectory at the spacecraft velocity. This represents the "raw" or uncorrected spectrum that enters the instrument apertures. The vertical line shows the approximate upper energy limit for ion detection by INMS.

pling was restricted to small periods over the north face of the ring plane and in the ring plane outside of the main rings. The sudden onset of the detected ions in the CAPS instrument measurements reported by Tokar et al. (2005) at about $z = +0.23\ R_S$ and $R = 1.86\ R_S$ requires a loss process like that described here for $R < R_x$ (e.g., the contours in the r–z plane in Figs. 6a and 6b are consistent with a steep onset). The energy spectra of the ions in Fig. 8a resemble those observed by CAPS during SOI (Tokar et al., 2005). In Fig. 11 we show a simulated energy spectrogram obtained by sampling the model ions along the SOI trajectory. This represents what would have been seen by an omnidirectional ion detector that made measurements through both the inbound and outbound legs of SOI, and whose measurements are corrected for the relative spacecraft motion (the energies are in the rest frame with respect to Saturn). The sharp cutoffs on either side of periapsis coincide with the edge of the ring source in our model ($\sim$2.4 R_S), as we do not consider any outward radial diffusion process(es). The intense portion of this simulated spectrogram on the outbound side (negative time) resembles the innermost portion of a similar CAPS spectrogram shown in Fig. 6 of Tokar et al. (2005). The detection of these ions by the INMS instrument with an upper energy limit for ion detection of $\sim$100 eV (in the space-

craft frame) sensitively depends on the relative motion of the spacecraft, which moves at ∼20 km/s during the period of the INMS observations of ring-related ions (Waite et al., 2005). To suggest how the model ionosphere spectrum would appear to INMS, we Doppler-shifted the model ion velocities along the spacecraft orbit to obtain the ion spectra shown in Fig. 12. It is clear that the INMS would be sensitive to a significant fraction of the ions encountered. The INMS also inferred the existence of shell or ring-like pitch angle distributions of the ions, consistent with Figs. 10a, 10b. Whether the SOI data allow detailed testing of such features is uncertain.

The potential implications of a successful model go well beyond the interpretation of SOI in situ data. The more spatially extended atomic oxygen torus observed by Cassini UVIS with peak emission around 3.8 R_S (Esposito et al., 2005) shows great temporal variability, implying both a changing source strength and effective removal. This torus must result in part from charge-exchange-neutralized oxygen ions from the ring ionosphere that have been accelerated by the corotation electric field (see Fig. 3b), and also from some ring atmosphere neutrals that have been scattered by the collisions onto elliptical orbits taking them to larger radii (e.g., Fig. 3 in Johnson et al., 2006). One can then ask whether an excitation radial profile (e.g., due to electron impact when the energetic magnetospheric electrons reappear outside the main rings) makes the UV torus peak at ∼3.8 R_S, rather than a source profile with a peak near Enceladus' orbit (at ∼3.9 R_S). CAPS electron measurements can help to answer this question. In other work, Krimigis et al. (2005) observe energetic neutral atoms escaping the Saturn environment after ions are injected into the inner magnetosphere—and charge exchange with the neutrals there. But the escaping energetic neutral atoms are only a small fraction of what might escape via the production of a ring ionosphere, which includes a percentage of all ions above the escape velocity (see Figs. 3a, 3b). Moreover, this escape and the ions precipitating into the atmosphere of Saturn may constitute an important loss process for ring material over time. As the Cassini Orbiter continues its tour of the Saturn system, we will better learn about the broader roles of the ring atmosphere and its ionosphere. Extensions of the model in which the neutral particles are also followed are planned as a follow-on to this work, with these continuing observations in mind.

Acknowledgments

The contributions to this work by J.G.L. and S.A.L. were supported by a subcontract award to the Space Sciences Laboratory, University of California, from the University of Michigan as part of the Cassini INMS Science Investigation contract from NASA/JPL.

References

Connerney, J.E.P., Acuna, M.H., Ness, N.F., 1983. Currents in Saturn's magnetosphere. J. Geophys. Res. 88, 8779–8789.

Dougherty, M.K., and 17 colleagues, 2005. Cassini magnetometer observations during Saturn orbit insertion. Science 307, 1266–1270.

Esposito, L.W., and 15 colleagues, 2005. Ultraviolet imaging spectroscopy shows an active saturnian system. Science 307, 1251–1255.

Hall, D.T., Strobel, D.F., Feldman, P.D., McGrath, M.A., Weaver, H.A., 1995. Detection of an oxygen atmosphere on Jupiter's moon Europa. Nature 373, 677–679.

Hansen, C.J., Shemansky, D.E., Hendrix, A.R., 2005. Cassini UVIS observations of Europa's oxygen atmosphere and torus. Icarus 176, 305–315.

Ip, W.-H., 1984. The ring atmosphere of Saturn: Monte Carlo simulations of the ring source model. J. Geophys. Res. 89, 8843–8849.

Ip, W.-H., 1995. Exospheric systems of Saturn's rings. Icarus 115, 295–303.

Johnson, R.E., Quickenden, T.I., Cooper, P.D., McKinley, A.J., Freeman, C., 2003. The production of oxidants in Europa's surface. Astrobiology 3, 823–850.

Johnson, R.E., Luhmann, J.G., Tokar, R.L., Bouhram, M., Berthelier, J.J., Sittler, E.C., Cooper, J.F., Hill, T.W., Crary, F.J., Young, D.T., 2006. Production, ionization and redistribution of Saturn's O_2 ring atmosphere. Icarus 180, 393–402.

Jurac, S., McGrath, M.A., Johnson, R.E., Richarson, J.D., Vasyliunas, V.M., Eviatar, A., 2002. Saturn: Search for a missing water source. Geophys. Res. Lett. 29, 1–4. 2172.

Krimigis, S.M., and 30 colleagues, 2005. Dynamics of Saturn's magnetosphere from MIMI during Cassini's orbital insertion. Science 307, 1270–1273.

Pospieszalska, M.K., Johnson, R.E., 1991. Micrometeorite erosion of the main rings as a source of plasma in the inner saturnian plasma torus. Icarus 93, 45–52.

Shemansky, D.E., Matheson, P., Hall, D.T., Hu, H.Y., Tripp, T.M., 1993. Detection of the hydroxyl radical in the Saturn magnetosphere. Nature 363, 329–331.

Shematovich, V.I., Johnson, R.E., Cooper, J.F., Wong, M.C., 2005. Surface-bounded atmosphere of Europa. Icarus 173, 480–498.

Tokar, R.L., Johnson, R.E., Thomsen, M.F., Dunlapp, D.M., Baragiola, R.A., Francis, M., Reisenfeld, D.B., Fish, B., Young, D.T., Crary, F.J., Coates, A.J., Gurnett, D.A., Kurth, W.S., 2005. Cassini observations of the thermal plasma in the vicinity of Saturn's main rings and the F and G rings. Geophys. Res. Lett. 32, 1–5. L14S04.

Waite, J.H., Cravens, T.E., Ip, W.-H., Kasprzak, W.T., Luhmann, J.G., McNutt, R.L., Niemann, H.B., Yelle, R.V., Mueller-Wodarg, I., Ledvina, S.A., Scherer, S., 2005. Cassini ion and neutral mass spectrometer measurements of oxygen ions near Saturn's A-ring. Science 307, 1260–1262.

Wilson, G.R., 1991. The plasma environment, charge state, and currents of Saturn's C and D rings. J. Geophys. Res. 96, 9689–9701.

Young, D.T., and 42 colleagues, 2005. Composition and dynamics of plasma in Saturn's magnetosphere. Science 307, 1262–1266.